

The railroad switch effect of seasonally reversing currents on the Bay of Bengal high salinity core

A. Sanchez-Franks¹, B. G. M. Webber^{2,3}, B. A. King¹, P. N. Vinayachandran⁴,
A. J. Matthews^{2,5}, P. M. F. Sheehan², A. Behara⁴, and C. P. Neema⁴

¹National Oceanography Centre, Southampton, United Kingdom

²Centre for Ocean and Atmospheric Sciences, School of Environmental Sciences, University of East Anglia, Norwich, United Kingdom

³Climatic Research Unit, University of East Anglia, Norwich, United Kingdom

⁴Centre for Atmospheric and Oceanic Sciences, Indian Institute of Science, Bangalore, India

⁵School of Mathematics, University of East Anglia, Norwich, United Kingdom

Key Points:

- The high salinity core observed in the Bay of Bengal during the southwest monsoon originates from the western equatorial Indian Ocean
- The Somali Current, Equatorial Undercurrent and Monsoon Current are key to supply and variability of the Bay of Bengal high salinity core
- Wind stress and El Niño determine the Equatorial Undercurrent velocity and thus the strength of the high salinity core on interannual scales

This article has been accepted for publication and undergone full peer review but has not been through the copyediting, typesetting, pagination and proofreading process which may lead to differences between this version and the Version of Record. Please cite this article as doi: [10.1029/2019GL082208](https://doi.org/10.1029/2019GL082208)

Corresponding author: A. Sanchez-Franks, alsf@noc.ac.uk

Abstract

The Southwest Monsoon Current (SMC) flows eastward from the Arabian Sea into the Bay of Bengal (BoB) during summer, advecting a core of high salinity water. This high salinity core has been linked with Arabian Sea High Salinity Water that is presumed to enter the BoB directly from the Arabian Sea via the SMC. Here we show that the high salinity core originates primarily from the western equatorial Indian Ocean, reaching the BoB via the Somali Current, the Equatorial Undercurrent and the SMC. Years with anomalously saline high salinity cores are linked with the East Africa Coastal Current and the Somali Current winter convergence, and an anomalously strong Equatorial Undercurrent. Seasonal reversals that occur at the Somali Current and SMC junctions act as railroad switches diverting water masses to different basins in the northern Indian Ocean. Interannual fluctuations of the Equatorial Undercurrent are linked to wind stress and El Niño.

Plain Language Summary

The northern Indian Ocean experiences a seasonal reversal of currents due to monsoon winds. During the summer, the monsoon current transports high salinity water from the Arabian Sea into the Bay of Bengal. This supply of salty water is believed to originate from the eastern Arabian Sea. Here we find that the intrusion of high salinity water originates instead from the western Arabian Sea. The origins of the high salinity water are traced to the western equatorial Indian Ocean via a seasonal equatorial undercurrent. In the western equatorial Indian Ocean there is a seasonal convergence of currents that is crucial to the supply of this salty water. Variability in the equatorial undercurrent is linked to wind fields and the El Niño Southern Oscillation. As a result, these findings shed new insight into which large-scale patterns influence the subsurface salinity in the Bay of Bengal that then modulate the variability of sea surface temperature and the strength of air-sea coupling in this region. Better representation of interaction between patterns of climate variability and the currents of the equatorial Indian Ocean could improve the representation of the Bay of Bengal in climate models and thus the representation of monsoon processes, including rainfall.

1 Introduction

One of the most remarkable characteristics of the northern Indian Ocean, that distinguishes it from any other ocean basin in the world, is the seasonal reversal of its major current systems. The South Asian monsoon dominates temporal variability of the surface circulation, leading to the reversal of the currents (Goswami, 2005; Shankar, Vinayachandran, & Unnikrishnan, 2002). In the western northern Indian Ocean, the Arabian Sea hosts the Somali Current that flows southward in boreal winter and northward in boreal summer (Schott & McCreary Jr, 2001). In the eastern northern Indian Ocean, the Bay of Bengal (BoB) is connected to the Arabian Sea via the Northeast Monsoon Current that flows westward from the BoB to the Arabian Sea during winter, and via the Southwest Monsoon Current (SMC) that flows eastward from the Arabian Sea to the BoB during summer (Schott & McCreary Jr, 2001). The monsoon currents can have a large impact on the distribution of northern Indian Ocean salinity (Vinayachandran, Masumoto, Mikawa, & Yamagata, 1999; Vinayachandran et al., 2013), which increases from east (i.e. BoB) to west (i.e. Arabian Sea). The Arabian Sea surface waters are highly saline due to strong evaporation (Antonov et al., 2010; Chatterjee et al., 2012), whereas the BoB is comparatively fresh at the surface due to the outflow from the Ganges-Brahmaputra and other river systems, and monsoon rainfall (Shetye et al., 1996; Vinayachandran, Murty, & Ramesh Babu, 2002).

One of the key features of the SMC is a core of high salinity water it advects into the BoB (Murty, Sarma, Rao, & Murty, 1992; Vinayachandran et al., 2013). The high salinity core (HSC) plays an important role in maintaining the BoBs salinity balance, as it is the main source of salinity available to balance the BoBs net outflow of freshwater (Schott, Xie, & McCreary, 2009; Vinayachandran et al., 1999, 2013). To date, several studies have linked the HSC to Arabian Sea High Salinity Water (ASHSW), which originates from the northern Arabian Sea and is transported to the BoB via the SMC (Jensen, 2001; Jensen et al., 2016; Schott & McCreary Jr, 2001; Vinayachandran et al., 1999; Webber et al., 2018).

Indian Ocean equatorial currents are also subject to the seasonal influence of the monsoon winds. Surface and subsurface eastward-flowing currents form, within the upper thermocline, along the Indian Ocean equator during the inter-monsoon periods (Schott & McCreary Jr, 2001; Wyrtki, 1973). At the surface, the narrow eastward current is known

79 as the Wyrтки Jet (Wyrтки, 1973), and below it lies the Indian Ocean Equatorial Under-
80 current (EUC) (Knauss & Taft, 1964; Nagura & McPhaden, 2016; Reppin, Schott, Fis-
81 cher, & Quadfasel, 1999; Schott & McCreary Jr, 2001). The equatorial currents connect
82 the western and eastern parts of the equatorial Indian Ocean and can have major im-
83 pacts on the transport and distribution of ocean heat (Reverdin, 1987; Wyrтки, 1973).
84 In this study, we focus on the subsurface current, the EUC, and demonstrate for the first
85 time a connection between the EUC and the BoB HSC. A new paradigm is presented
86 to explain the source, pathways and variability of the BoB HSC. Driving mechanisms
87 for fluctuations of the EUC and BoB HSC on interannual time scales are also explored.

88 **2 Data and Methods**

89 For this study, the Nucleus for European Modelling of the Ocean (NEMO) version
90 3.1 (Madec, 2008) estimates of velocity and salinity were used. NEMO is a global ocean
91 model (analysis and forecasting system) with a resolution of $1/12^\circ$ in the horizontal and
92 50 levels in the vertical, with 1 m resolution at the surface, increasing to 450 m near the
93 bottom (5500 m). Surface forcing is from operational forecasts of the European Centre
94 for Medium-Range Weather Forecasts (ECMWF). NEMO assimilates a combination of
95 observational datasets (satellite and in situ).

96 NEMO was compared with a product constructed from optimally interpolated (OI)
97 profiles of Argo floats. The OI mapping is constructed based on anomalies relative to
98 a reference ocean, from the monthly World Ocean Atlas climatology (Boyer et al., 2013).
99 Data are gridded at 25 longitude grid points at 0.5° intervals, and days are centred on
100 midnight UTC with a window of ± 0.5 days. More details on this product and the method
101 are described in (Desbruyeres, McDonagh, King, & Thierry, 2017).

102 The wind field is investigated using TropFlux zonal wind stress (B. P. Kumar, Vialard,
103 Lengaigne, Murty, & Mcphaden, 2012). In the tropical Indian Ocean, a region of sparse
104 data and large model biases, TropFlux has been shown to outperform other reanalysis
105 products (Sanchez-Franks et al., 2018). The Indian Ocean Dipole (IOD) is quantified as
106 the difference between sea surface temperature (SST) anomalies in the western (50°E -
107 70°E , 10°S - 10°N) and eastern (90°E - 110°E , 10°S - 0°N) equatorial Indian Ocean (Saji,
108 Goswami, Vinayachandran, & Yamagata, 1999). Weekly values of the Dipole Mode In-
109 dex and the oceanic Nino3.4 El Niño index (the SST anomaly for the region: 5°N - 5°S

110 and 170-120°W) are interpolated to daily resolution for comparison with the NEMO daily
111 product. Both indices are based on the weekly updated Reynolds OIv2 SST analysis (Reynolds,
112 Rayner, Smith, Stokes, & Wang, 2002).

113 All data have daily resolution (or interpolated to daily resolution where needed)
114 for the years 2007 to 2016, and a 61-day smoothing has been applied to all variables to
115 reduce noise associated with high-frequency variability.

116 **3 The Bay of Bengal high salinity core**

117 The NEMO subsurface salinity anomalies along 7°N show the HSC as a recurring
118 annual feature with positive salinity anomalies appearing during boreal summer (Fig. 1a).
119 Very high salinity anomalies (≥ 0.15), representative of an unusually strong HSC, are
120 observed during the summers of 2007, 2014 and 2016, and to a lesser extent during 2012
121 and 2013 (Fig. 1a). Zero or negative salinity anomalies are observed during the summers
122 of 2010 and 2015 (Fig. 1a). The structure of the subsurface (90-130 m) salinity across
123 the wider BoB during the summer of 2014 (Fig. 1b) shows the intrusion of a high salin-
124 ity tongue alongside the eastward flowing SMC (surface current vectors from OSCAR;
125 Bonjean and Lagerloef (2002)), in agreement with Vinayachandran et al. (2018, 2013)
126 and Webber et al. (2018). The SMC is a surface-intensified current with northward flow
127 extending to a depth of 300 meters (Vinayachandran et al., 2018; Webber et al., 2018).
128 As the HSC is advected north by the SMC, it is subducted under the fresher, lighter wa-
129 ters of the northern BoB (Vinayachandran et al., 1999, 2013). Changes to the HSC may
130 also occur from the surface flows of saline waters being subducted (Vinayachandran et
131 al., 2013).

132 A comparison of the cross sections of the vertical structure of salinity at 7°N from
133 NEMO (Fig. 1 d,e) and the Argo OI (not shown) show the model agrees well with the
134 observations. Both NEMO (Fig. 1d) and the Argo OI show the structure of the HSC ($> 35 \text{ g kg}^{-1}$)
135 centred between 75 and 130 m and 85°E to 90°E for summer 2014 (Fig. 1d) and 83°E
136 to 87°E for the summer of 2015 (Fig. 1e), consistent with previous studies (Vinayachan-
137 dran et al., 2013; Webber et al., 2018). Webber et al. (2018) found that the NEMO ocean
138 model provides an accurate representation of the velocity, salinity and density structure
139 in the BoB, compared to observations made during the 2016 monsoon season that were
140 not assimilated into the model (Fig. 2 of Webber et al. (2018)). We note NEMO shows

141 a more defined salinity core structure and higher values for the HSC than the Argo OI.
142 This can primarily be attributed to the low spatial and temporal resolution of the Argo
143 OI product.

144 The HSC is a pervasive feature in the southern BoB that occurs alongside the SMC.
145 We note the relationship between the strength of the SMC and variability in the HSC
146 appears weak (Fig. S1). Spatial variability of the HSC is large (Fig. 1a) and changes in
147 isopycnal depth (heave) are substantial. The salinity core typically rests on the 1024 kg m^{-3}
148 isopycnal (Fig. 1d,e), which is within the known density range ($1022.8 - 1024 \text{ kg m}^{-3}$)
149 for the ASHSW (Shenoi, Shetye, Gouveia, & Michael, 1993). Therefore model salinity
150 and velocity are mapped onto the 1024 kg m^{-3} isopycnal to trace the pathways of this
151 water mass.

152 **4 The western equatorial Indian Ocean origins of the high salinity core**

153

154 To trace the origins of the HSC, a backwards trajectory particle experiment was
155 conducted. NEMO velocities were interpolated to the 1024 kg m^{-3} isopycnal surface (ap-
156 proximately 80-100 m depth across most of the Indian Ocean (Fig. S2)). Particles were
157 then tracked backwards in time along this surface, neglecting diapycnal diffusivity, which
158 we assume would have a small impact on the backward trajectories on time periods less
159 than 1 year. Model velocities on this isopycnal surface were bilinearly interpolated to
160 the particle locations, and the particles were advected using a fourth-order Runge-Kutta
161 scheme with a time step of 1 hour. This time step is chosen to avoid particles crossing
162 multiple grid boxes within a single time step. To track the origin of water masses that
163 pass through 7°N during the southwest monsoon, particles are released at 5-day inter-
164 vals from 1 June to 30 August along 7°N (between 82°E and 90°E) and are tracked back-
165 wards to 1 January. This experiment is repeated for anomalously high/low HSC at 7°N
166 (see below). Similar backwards tracking experiments have been shown in Jensen (2003).

167 Figure 2 shows that during anomalously high salinity years (2007, 2014 and 2016),
168 highly saline ($> 35 \text{ g kg}^{-1}$) particles predominantly originate from the western equato-
169 rial Indian Ocean via the equatorial current and the Somali Current to the north and,
170 to a lesser extent, the East African Coastal Current (EACC) to the south; whereas fresher
171 ($< 35 \text{ g kg}^{-1}$) particles originate from interior BoB recirculation (Fig. 2a). The main
172 source of high salinity in the western equatorial Indian Ocean, consistent with Fig. 2a,

173 is the Somali Current. Note that the colour of each line only represents the salinity of
174 the particle along 7°N and does not account for any change in salinity along the track.
175 During winter the southward Somali Current advects highly saline ($> 36 \text{ g kg}^{-1}$) wa-
176 ters from the western Arabian Sea (Antonov et al., 2010; Chatterjee et al., 2012; S. P. Ku-
177 mar & Prasad, 1999), converges with the EACC and feeds into the eastward equatorial
178 currents (Schott & McCreary Jr, 2001). During the summer monsoon, however, the So-
179 mali Current flows north, diverting the waters from the EACC toward the Arabian Sea
180 and away from the equatorial currents (Wyrski, 1973). The 8 month time period observed
181 for the anomalously saline HSC particles initialised in Jul-Aug in the BoB places their
182 origins in the western Indian Ocean in winter of the previous year. This suggests that
183 the high salinity water originates from the EACC and Somali Current confluence zone
184 that occurs in winter (Fig. 2a). Given that ASHSW is in the $1022.8 - 1024 \text{ kg m}^{-3}$ den-
185 sity range (Shenoi et al., 1993) and that anticyclonic circulation advects the ASHSW from
186 the northern to the southwestern Arabian Sea (Prasad & Ikeda, 2002), it is likely that
187 some of the source water mass is ASHSW.

188 Conversely, during the anomalously fresh HSC years (2008, 2010 and 2015), there
189 are significantly fewer high salinity ($> 35 \text{ g kg}^{-1}$) particles and fewer trajectories along
190 the equator (Fig. 2b). In the space of 6-8 months most particles only travel eastwards
191 from 55°E (Fig. 2b); it takes over 1 year for them to be traced back to the western equa-
192 torial Indian Ocean (not shown), suggesting that they would have originated from the
193 western equatorial Indian Ocean during the previous summer, when the Somali Current
194 was flowing north. Composites of velocity on the 1024 kg m^{-3} isopycnal surface show
195 that the velocity of the equatorial currents is significantly higher during the anomalously
196 saline HSC years compared with the anomalously fresh HSC years (Fig. S2). Slower ad-
197 vection would also allow a longer period for isopycnal mixing to further reduce salinity.
198 At the western boundary instabilities generated by the southern gyre (Kindle & Thomp-
199 son, 1989) may also contribute to strong water mass mixing.

200 Sensitivity tests for density class choice and a forward trajectory experiment were
201 also run. The sensitivity test for density class was run using the backwards trajectory
202 particle experiment for 1023 kg m^{-3} and 1025 kg m^{-3} isopycnals. Compared to 1024 kg m^{-3}
203 run, both runs show significantly fewer particles originating from the western Arabian
204 Sea (i.e. via the Somali Current)(Fig. S3). The run for 1023 kg m^{-3} surface also sug-
205 gests more particles originate from the eastern Arabian Sea for water masses lighter than

206 the HSC (Fig. S3, 1d,e). The forward trajectory particle experiment was initiated from
207 a section between 50-55°E along 10°N in the western Arabian Sea every 5 days from 1
208 December the previous year until 30 January the current year, and then run forwards
209 until 30 August. (Fig. S4). This run confirmed that during the high-salinity years, a large
210 number of particles from the western Arabian Sea reached the BoB (Fig. S4a), partic-
211 ularly in contrast to the low-salinity years (Fig. S4b).

212 These results suggest the following key points: 1) Most of the HSC water originates
213 from the western equatorial Indian Ocean and the western Arabian Sea is an important
214 source region, 2) the HSC is more likely related to the pathways of the currents rather
215 than transformation or changing properties in the source region, and 3) the existence of
216 an anomalously saline HSC is linked to the equatorial currents velocity required to trans-
217 port highly saline waters from the winter western Indian Ocean convergence zone in the
218 time for the BoB summer monsoon.

19 **5 Variability and mechanisms for the high salinity core and the equa-** 220 **torial currents**

221 The connection between the HSC in the BoB at 7°N and the equatorial currents
222 is investigated through analysis of NEMO currents and salinity from a section along 65°E
223 between 2°S to 1.5°N (Fig. 2; magenta line perpendicular to the equator). The eastward
224 velocity of the equatorial current is centred subsurface (50-130 m) around the equator
225 and experiences a biannual strengthening in speed (Fig. 3a; Fig. S5), associated with the
226 spring (Feb-Apr) and fall (Sept) EUC generated from the inter-monsoon wind regimes
227 (Chen, Han, Li, Wang, & McPhaden, 2015; Knauss & Taft, 1964; Nagura & McPhaden,
228 2016; Reppin et al., 1999). On average, the simulated speeds of the EUC appear to be
229 0.5 m s^{-1} during their peak in the spring season (Fig. S5), in agreement with observa-
230 tions shown in Nagura and McPhaden (2016). This spring peak is associated with a cli-
231 matological subsurface salinity maximum (Fig. S5). Anomalously high speeds ($> 0.5 \text{ m s}^{-1}$),
232 peaking at the 1024 kg m^{-3} isopycnal are observed during the spring (Feb-Apr) inter-
233 monsoon periods of 2007, 2014 and 2016 at 65°E (Fig. 3a; green contourlines and red
234 bars) in agreement with the years with anomalously saline HSC in the BoB (Sections
235 3 and 4). Similarly, anomalously high salinity ($> 35.2 \text{ g kg}^{-1}$) is observed a few months
236 later (Jun-Sept) between 83°E and 90°E in the southern BoB (7°N) for the same years
237 (Fig. 3b; magenta contourlines and red bars). Years flagged as anomalously low for salin-

ity in the BoB (2008, 2010 and 2015; see Fig. 1 and Fig. 2) show comparatively weaker eastward velocities and corresponding lower salinity in the southern BoB (Fig. 3a,b).

Comparison of the eastward velocity at 65°E and the salinity at 7°N clearly shows peaks in BoB salinity are preceded (by a few months) by a peak in eastward velocity at 65°E, associated with an anomalously strong spring EUC (Fig. 3c). Further, the annually averaged spring EUC (fall EUC is excluded as it has no bearing on the summer BoB salinity) compared with the summer (June-Aug) BoB salinity shows a correlation of 0.74 significant at the 95% level (Fig. 3e). Notable exceptions occur during 2012, when a peak in salinity was not accompanied by a peak in EUC velocity (Fig. 3e). The higher salinity apparent during that year may have originated from the eastern Arabian Sea, or it may have been a result of higher salinity particles that accumulated in the eastern equatorial Indian Ocean the year before. In general, a strong spring EUC transports the highly saline waters of the winter EACC/Somali Current convergence zone in time for the SMC to advect an anomalously saline HSC into the BoB.

To investigate the mechanisms driving variability in EUC velocity, we examine the equatorial zonal wind stress, the Indian Ocean Dipole (IOD) and the El Niño Southern Oscillation (ENSO). Firstly, the wind stress is examined as the EUC has been shown to be a response to the inter-monsoon wind regimes, and in particular to the zonal wind stress along the equator (Chen et al., 2015; Nagura & McPhaden, 2010, 2016). Here, TropFlux Zonal Wind stress is averaged over 2°S-2°N and 60°E-90°E. The EUC also has a connection with the IOD (Chen et al., 2015; Zhang, McPhaden, & Lee, 2014), where positive (negative) IOD events represent warm SST anomalies in the western (eastern) Indian Ocean (Yamagata et al., 2004).

Wind stress, the IOD and ENSO are compared with the eastward velocity at 65°E. All three parameters experience similar biannual variability (Fig. 3c,d). A lag correlation shows that zonal wind stress leads EUC eastward velocity by 62 days ($r=-0.63$, $p<0.05$) suggesting that decreases (increases) in easterly winds results in the strengthening (weakening) of the EUC eastward velocity. To investigate the link between the EUC and the IOD and ENSO, all three parameters were annually averaged. ENSO leads EUC variability by 1 year ($r=0.79$, $p<0.05$) (Fig. 3f). In contrast, the link between the IOD and the EUC velocity is not as robust ($r=-0.40$, $p<0.20$). In general, positive (negative) ENSO results in the strengthening (weakening) of the EUC eastward velocity. It is somewhat

270 surprising that ENSO rather than the IOD dominates the variability of the velocity at
271 65°E, as the IOD has been shown to dominate the equatorial Indian Ocean (Yu, Xiang,
272 Liu, & Liu, 2005). It is possible that the discrepancy lies in the selected region at 65°E,
273 which is a bit further west of the centers of action depicted in Yu et al. (2005). We also
274 note that 2007 and 2014-2016 were El Niño years.

275 **6 The railroad switch effect of the Indian Oceans seasonally revers-** 276 **ing currents**

277 We have shown thus far that the inflow of high salinity water into the BoB has its
278 origins in the western equatorial Indian Ocean and that water mass pathways are the
279 key drivers of changes in the BoBs HSC (Sections 4 and 5). Results presented here have
280 also underlined the importance of the seasonal reversals of the Somali Current, the SMC
281 and the EUC as key players on pathways and terminus of high salinity particles origi-
282 nating from the western Indian Ocean. Based on this, we postulate that there are two
283 key junctions in the water mass pathways: one in the west with the EACC and the So-
284 mali Current and another just south of Sri Lanka with the EUC and the Monsoon Cur-
285 rent. Depending on the time of year, the current reversals that occur at these junctions
286 act as railroad switches (or points on the British railway system) diverting water masses
287 to different destinations in the northern Indian Ocean. Here, we outline the four such
288 possible railroad track circulation scenarios and the resulting impact on salinity distri-
289 bution across the northern Indian Ocean and, in particular, the BoB.

290 In boreal winter, the Somali Current flows south advecting the highly saline wa-
291 ters of the western Arabian Sea toward the northward flowing EACC feeding into the
292 South Equatorial Counter Current (Schott et al., 2009) and [eventually] the springtime
293 EUC (Fig. 4a,b; Fig. S6a). During the spring inter-monsoon period (Feb-Apr), the EUC
294 forms and transports waters from the west to the east equatorial Indian Ocean (Chen
295 et al., 2015) (Fig. S6b,c). Section 4 showed that when the EUC is anomalously strong,
296 the time it takes to advect waters from the western to the eastern equatorial Indian Ocean
297 is approximately 8 months (Fig. 2). Hence, for a strong spring EUC, highly saline wa-
298 ters from the wintertime EACC and Somali Current convergence zone reach the east-
299 ern equatorial Indian Ocean in time to make the connection with the eastward flowing
300 SMC, which advects those highly saline waters into the BoB (Fig. 4a; Fig. S6a,b,d). Con-
301 versely, if the EUC is not anomalously strong, it may take over a year for the highly saline

302 waters of the winter EACC and the Somali Current convergence zone to reach the BoB
303 (Fig. 4b; Fig. S6c,e). By then isopycnal mixing may have diluted the waters and the SMC
304 will have reversed (i.e. to the Northeast Monsoon Current), with fresher BoB waters flow-
305 ing westward toward the Arabian Sea (Fig. 4b).

306 In boreal summer, some the EACC flow is diverted north into the northward flow-
307 ing Somali Current, cutting of the supply of highly saline Arabian Sea waters from the
308 EUC (Fig. 4c,d). In these scenarios the strength of the EUC is irrelevant as there is less
309 highly saline water available for it to transport eastwards regardless.

10 **7 Summarising Remarks**

11 The summer monsoon HSC in the BoB is the main source of salinity that balances
312 the BoBs freshwater export (Vinayachandran et al., 1999, 2013). The source of this salin-
13 ity has been linked to the ASHSW, which forms in the northern Arabian Sea, and is pre-
314 sumed to enter the BoB via the eastern Arabian Sea and the SMC (Jensen, 2001; Jensen
15 et al., 2016; Schott & McCreary Jr, 2001; Vinayachandran et al., 1999). In this study
16 a new paradigm is presented to explain the origins and variability of the BoB HSC, stat-
317 ing chiefly that 1) the BoB HSC primarily originates from the western equatorial Indian
18 Ocean and, in particular, the western Arabian Sea is a key source region; 2) water mass
319 pathways rather than transformation are key source of changes in the HSC; 3) the key
320 pathways are dominated by the Somali Current, the EUC and the SMC; 4) the anoma-
321 lously saline BoB HSC is linked to an anomalously strong spring EUC and 5) interan-
322 nual variability in the EUC is shown to be dominated by zonal wind stress and ENSO.
323 Given that the salinity stratification in the BoB is a crucial factor in the distribution (Shenoi,
24 Shankar, & Shetye, 2002) and variability (Li, Han, Wang, & Ravichandran, 2016) of mon-
325 soon rainfall, our findings demonstrate a new oceanic mechanism through which ENSO
26 and equatorial current dynamics will influence the rainfall of the South Asian monsoon.

36 **Acknowledgments**

357 The NERC Bay of Bengal Boundary Layer Experiment (BoBBLE) project supported
358 ASF and BAK (NE/L013835/1), BGMW and PMFS (NE/L013827/1). PNV, AB and
359 CPN are supported by the Indian BoBBLE program funded by the Ministry of Earth
360 Sciences, government of India, under its Monsoon Mission program administered by the
361 Indian Institute of Tropical Meteorology, Pune. The authors would also like to acknowl-

edge the Copernicus Marine Environment Monitoring Service for NEMO data access available here: <http://marine.copernicus.eu/services-portfolio/access-to-products/>, the International Argo Program for Argo data access (<http://argo.jcommops.org>), ESSO-INCOIS for TropFlux data access (<http://www.incois.gov.in/tropflux/>), the National Oceanic and Atmospheric Administration (NOAA) for ENSO data access (<http://www.cpc.ncep.noaa.gov/data/indices/>) and Dipole Mode Index data access (<https://stateoftheocean.osmc.noaa.gov/sur/ind/dmi.php>). The authors are also grateful for the helpful insight and comments from two anonymous reviewers.

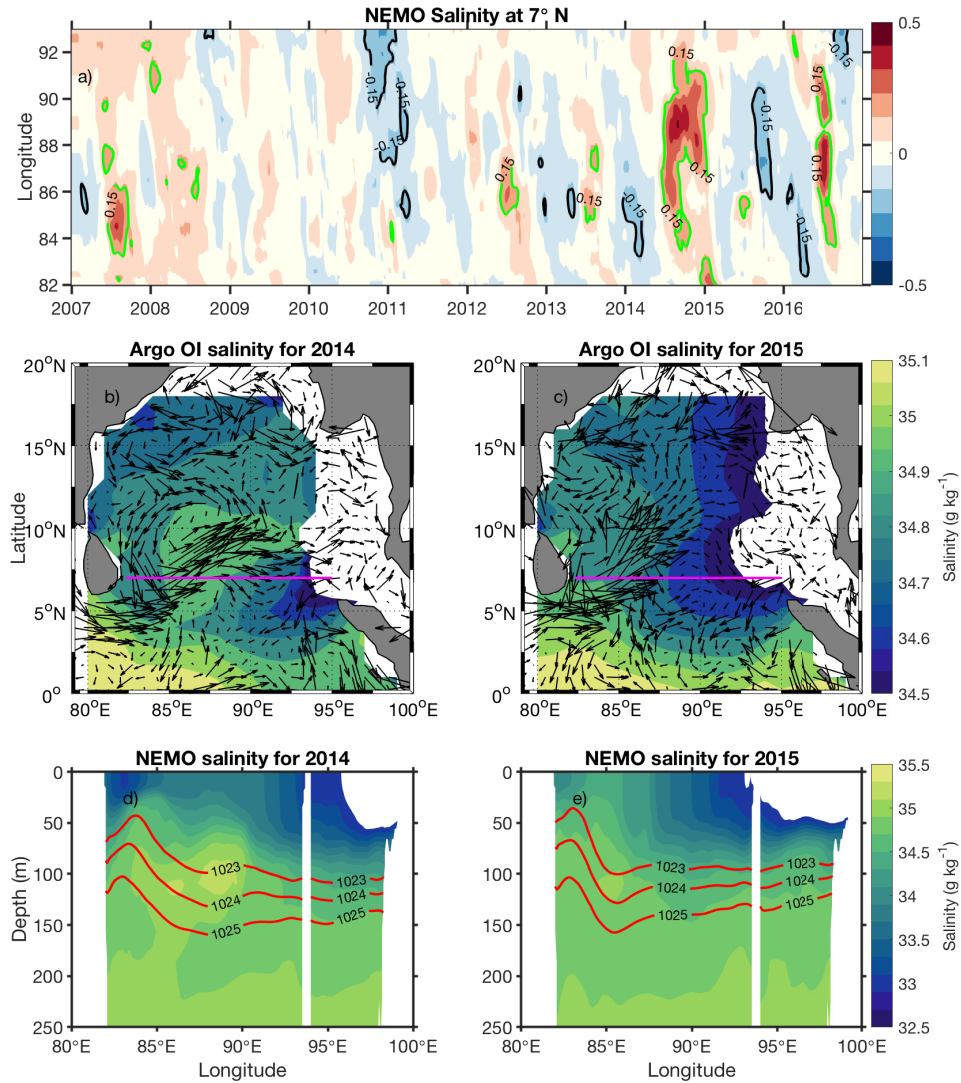
References

- Antonov, J., Seidov, D., Boyer, T., Locarnini, R., Mishonov, A., Garcia, H., . . . Johnson, D. (2010). World ocean atlas 2009, vol. 2, salinity, edited by S. Levitus, 184 pp [Journal Article]. *US Gov. Print. Off., Washington, DC*.
- Bonjean, F., & Lagerloef, G. S. (2002). Diagnostic model and analysis of the surface currents in the tropical Pacific ocean [Journal Article]. *Journal of Physical Oceanography*, *32*(10), 2938-2954.
- Boyer, T. P., Antonov, J. I., Baranova, O. K., Coleman, C., Garcia, H. E., Grodsky, A., . . . O'Brien, T. D. (2013). World ocean database 2013 [Journal Article].
- Chatterjee, A., Shankar, D., Shenoi, S., Reddy, G., Michael, G., Ravichandran, M., . . . Sanjeevan, V. (2012). A new atlas of temperature and salinity for the north Indian ocean [Journal Article]. *Journal of Earth System Science*, *121*(3), 559-593.
- Chen, G., Han, W., Li, Y., Wang, D., & McPhaden, M. J. (2015). Seasonal-to-interannual time-scale dynamics of the equatorial undercurrent in the Indian ocean. *Journal of Physical Oceanography*, *45*(6), 1532-1553.
- Desbruyeres, D., McDonagh, E. L., King, B. A., & Thierry, V. (2017). Global and full-depth ocean temperature trends during the early twenty-first century from Argo and repeat hydrography [Journal Article]. *Journal of Climate*, *30*(6), 1985-1997.
- Goswami, B. N. (2005). *South Asian monsoon* [Book]. Springer.
- Jensen, T. G. (2001). Arabian sea and bay of Bengal exchange of salt and tracers in an ocean model [Journal Article]. *Geophysical Research Letters*, *28*(20), 3967-3970.

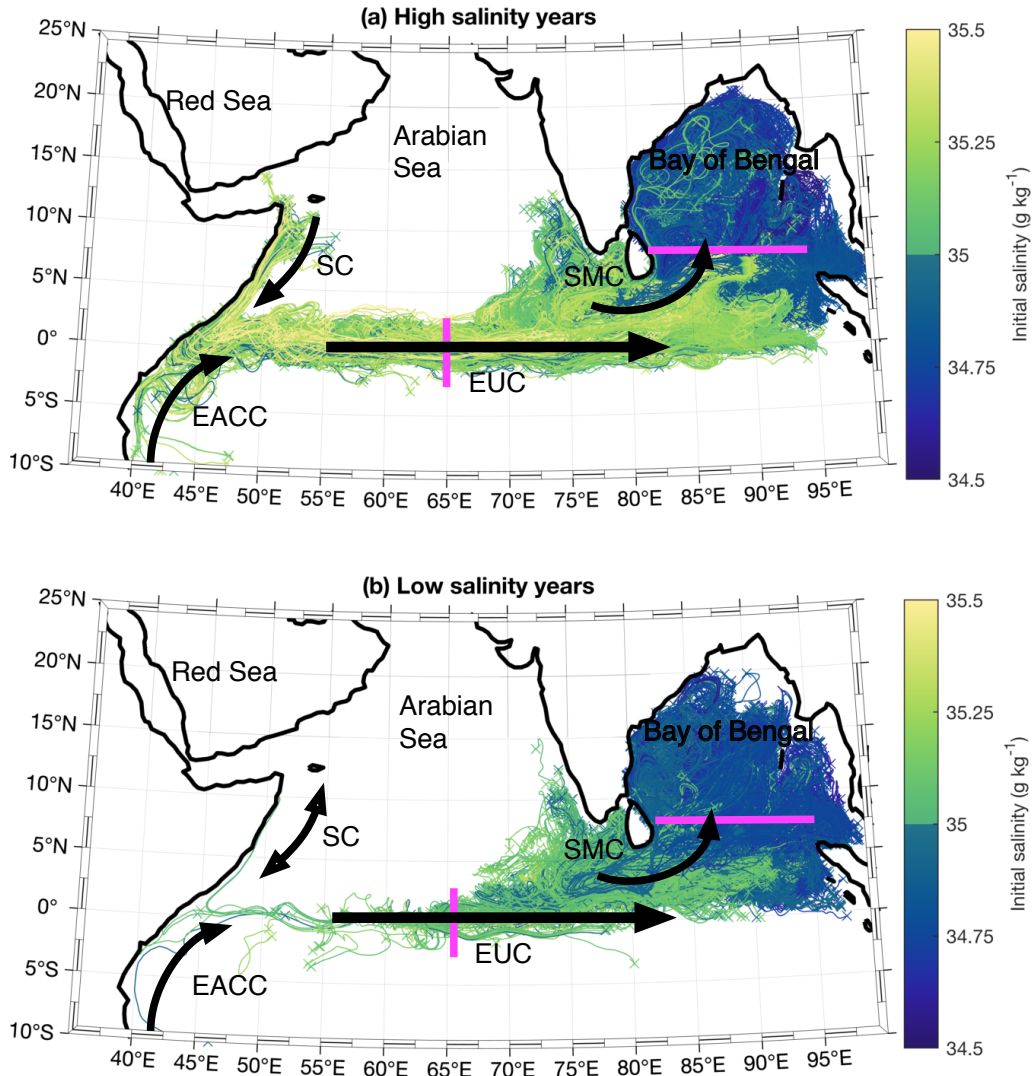
- 394 Jensen, T. G., Wijesekera, H. W., Nyadjro, E. S., Thoppil, P. G., Shriver, J. F.,
 395 Sandeep, K., & Pant, V. (2016). Modeling salinity exchanges between the
 396 equatorial indian ocean and the bay of bengal [Journal Article]. *Oceanography*,
 397 *29*(2), 92-101.
- 398 Kindle, J. C., & Thompson, J. D. (1989). The 26-and 50-day oscillations in the
 399 western indian ocean: Model results. *Journal of Geophysical Research: Oceans*,
 400 *94*(C4), 4721-4736.
- 401 Knauss, J. A., & Taft, B. A. (1964). Equatorial undercurrent of the indian ocean.
 402 *Science*, *143*(3604), 354-356.
- 403 Kumar, B. P., Vialard, J., Lengaigne, M., Murty, V., & Mcphaden, M. J. (2012).
 404 Tropflux: air-sea fluxes for the global tropical oceansdescription and evaluation
 405 [Journal Article]. *Climate Dynamics*, *38*(7-8), 1521-1543.
- 406 Kumar, S. P., & Prasad, T. (1999). Formation and spreading of arabian sea high-
 407 salinity water mass [Journal Article]. *Journal of Geophysical Research: Oceans*,
 408 *104*(C1), 1455-1464.
- 409 Li, Y., Han, W., Wang, W., & Ravichandran, M. (2016). Intraseasonal variability
 410 of sst and precipitation in the arabian sea during the indian summer monsoon:
 411 Impact of ocean mixed layer depth [Journal Article]. *Journal of Climate*,
 412 *29*(21), 7889-7910.
- 413 Madec, G. (2008). *Nemo, the ocean engine, note du pole de modelisation, insti-*
 414 *tut pierre-simon laplace (ipsl), france, no 27 issn no 12881619* [Generic]. Tech.
 415 rep.
- 416 Murty, V., Sarma, Y., Rao, D., & Murty, C. (1992). Water characteristics, mix-
 417 ing and circulation in the bay of bengal during southwest monsoon [Journal
 418 Article]. *Journal of Marine Research*, *50*(2), 207-228.
- 419 Nagura, M., & McPhaden, M. J. (2010). Wyrтки jet dynamics: Seasonal variability
 420 [Journal Article]. *Journal of Geophysical Research: Oceans*, *115*(C7).
- 421 Nagura, M., & McPhaden, M. J. (2016). Zonal propagation of near-surface zonal
 422 currents in relation to surface wind forcing in the equatorial indian ocean.
 423 *Journal of Physical Oceanography*, *46*(12), 3623-3638.
- 424 Prasad, T., & Ikeda, M. (2002). A numerical study of the seasonal variability of
 425 arabian sea high-salinity water. *Journal of Geophysical Research: Oceans*,
 426 *107*(C11).

- 427 Reppin, J., Schott, F. A., Fischer, J., & Quadfasel, D. (1999). Equatorial cur-
428 rents and transports in the upper central indian ocean: Annual cycle and
429 interannual variability. *Journal of Geophysical Research: Oceans*, *104*(C7),
430 15495–15514.
- 431 Reverdin, G. (1987). The upper equatorial indian ocean. the climatological seasonal
432 cycle [Journal Article]. *Journal of Physical Oceanography*, *17*(7), 903-927.
- 433 Reynolds, R. W., Rayner, N. A., Smith, T. M., Stokes, D. C., & Wang, W. (2002).
434 An improved in situ and satellite sst analysis for climate. *Journal of climate*,
435 *15*(13), 1609–1625.
- 436 Saji, N., Goswami, B., Vinayachandran, P., & Yamagata, T. (1999). A dipole mode
437 in the tropical indian ocean [Journal Article]. *Nature*, *401*(6751), 360. Re-
438 trieved from <https://www.nature.com/articles/43854.pdf>
- 439 Sanchez-Franks, A., Kent, E. C., Matthews, A. J., Webber, B. G. M., Peatman,
440 S. C., & Vinayachandran, P. N. (2018). Intraseasonal variability of air-sea
441 fluxes over the bay of bengal during the southwest monsoon [Journal Article].
442 *Journal of Climate*.
- 443 Schott, F. A., & McCreary Jr, J. P. (2001). The monsoon circulation of the indian
444 ocean [Journal Article]. *Progress in Oceanography*, *51*(1), 1-123.
- 445 Schott, F. A., Xie, S., & McCreary, J. P. (2009). Indian ocean circulation and cli-
446 mate variability [Journal Article]. *Reviews of Geophysics*, *47*(1).
- 447 Shankar, D., Vinayachandran, P., & Unnikrishnan, A. (2002). The monsoon currents
448 in the north indian ocean [Journal Article]. *Progress in oceanography*, *52*(1),
63-120.
- 450 Shenoi, S., Shankar, D., & Shetye, S. (2002). Differences in heat budgets of the
451 nearsurface arabian sea and bay of bengal: Implications for the summer mon-
452 soon [Journal Article]. *Journal of Geophysical Research: Oceans*, *107*(C6),
453 5-1-5-14.
- 454 Shenoi, S., Shetye, S., Gouveia, A., & Michael, G. (1993). Salinity extrema in the
455 arabian sea. *Mitt. Geol.Palaontol. University of Hamburg, Germany*.
- 456 Shetye, S., Gouveia, A., Shankar, D., Shenoi, S., Vinayachandran, P., Sundar, D., ...
457 Nampoothiri, G. (1996). Hydrography and circulation in the western bay of
458 bengal during the northeast monsoon [Journal Article]. *Journal of Geophysical
459 Research: Oceans*, *101*(C6), 14011-14025.

- 460 Vinayachandran, P., Masumoto, Y., Mikawa, T., & Yamagata, T. (1999). Intrusion
51 of the southwest monsoon current into the bay of bengal [Journal Article].
462 *Journal of Geophysical Research: Oceans*, *104*(C5), 11077-11085.
- 463 Vinayachandran, P., Matthews, A. J., Vijay Kumar, K., Sanchez-Franks, A.,
464 Thushara, V., George, J., ... Roy, R. (2018). Bobble (bay of bengal bound-
465 ary layer experiment): Oceanatmosphere interaction and its impact on the
466 south asian monsoon [Journal Article]. *Bulletin of the American Meteorological*
467 *Society*(2018).
- 468 Vinayachandran, P., Murty, V., & Ramesh Babu, V. (2002). Observations of barrier
469 layer formation in the bay of bengal during summer monsoon [Journal Article].
470 *Journal of Geophysical Research: Oceans*, *107*(C12), SRF 19-1-SRF 19-9.
- 471 Vinayachandran, P., Shankar, D., Vernekar, S., Sandeep, K., Amol, P., Neema, C.,
472 & Chatterjee, A. (2013). A summer monsoon pump to keep the bay of bengal
473 salty [Journal Article]. *Geophysical Research Letters*, *40*(9), 1777-1782.
- 474 Webber, B. G. M., Matthews, A. J., Vinayachandran, P. N., Neema, C. P., Sanchez-
475 Franks, A., Vijith, V., ... Baranowski, D. B. (2018). The dynamics of the
476 southwest monsoon current in 2016 from high-resolution in situ observations
477 and models [Journal Article]. *Journal of Physical Oceanography*, *48*(10), 2259-
478 2282. Retrieved from <https://doi.org/10.1175/JPO-D-17-0215.1> doi:
479 10.1175/JPO-D-17-0215.1
- 480 Wyrki, K. (1973). An equatorial jet in the indian ocean [Journal Article]. *Sci-*
481 *ence*, *181*(4096), 262-264. Retrieved from [http://science.sciencemag.org/](http://science.sciencemag.org/content/sci/181/4096/262.full.pdf)
482 [content/sci/181/4096/262.full.pdf](http://science.sciencemag.org/content/sci/181/4096/262.full.pdf)
- 483 Yamagata, T., Behera, S. K., Luo, J.-J., Masson, S., Jury, M. R., & Rao, S. A.
484 (2004). Coupled ocean-atmosphere variability in the tropical indian ocean
485 [Journal Article]. *Earths Climate: The OceanAtmosphere Interaction, Geophys.*
486 *Monogr*, *147*, 189-212.
- 487 Yu, W., Xiang, B., Liu, L., & Liu, N. (2005). Understanding the origins of interan-
488 nual thermocline variations in the tropical indian ocean. *Geophysical research*
489 *letters*, *32*(24).
- 490 Zhang, D., McPhaden, M. J., & Lee, T. (2014). Observed interannual variability of
491 zonal currents in the equatorial indian ocean thermocline and their relation to
492 indian ocean dipole. *Geophysical Research Letters*, *41*(22), 7933-7941.



327 **Figure 1.** Salinity in the Bay of Bengal at 7°N for (a) NEMO subsurface (110-130 m) salinity
 328 anomalies (from long term mean) with 61-day smoothing applied from 2007 to 2016; (b) OSCAR
 329 surface current velocities (vector) and Argo optimally interpolated (OI) subsurface (110-130 m)
 330 salinity (shaded) during anomalously high HSC summer (JAS) 2014 and (c) anomalously low
 331 HSC summer 2015; (d) NEMO vertical cross sections of salinity at 7°N during anomalously high
 332 HSC summer 2014 and (e) anomalously low HSC summer 2015. Magenta line (b,c) indicates
 333 location of vertical cross section. Red lines (d,e) indicates the location of the 1023, 1024 and 1025
 334 kg m⁻³ isopycnal.



335 **Figure 2.** Composite of NEMO salinity particles released at 82-90°E, 7°N at 5-day intervals
 336 from 1 June to 30 August and tracked backward to 1 January for high salinity years (2007, 2014
 337 and 2016) and low salinity years (2008, 2010 and 2015) on the 1024 kg m⁻³ isopycnal. Magenta
 338 lines indicate regions where the Equatorial Undercurrent (EUC) and the Bay of Bengal high
 339 salinity core were measured. SC = Somali Current, EACC = East African Coastal Current, SMC
 340 = Southwest Monsoon Current.

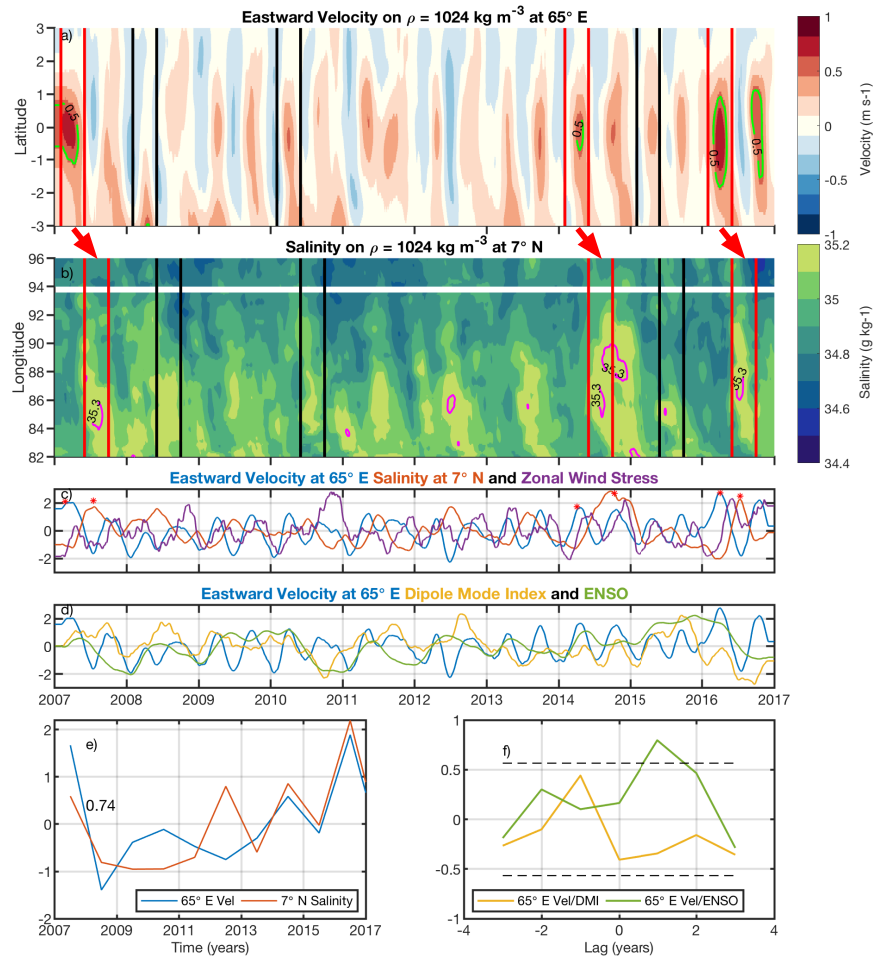
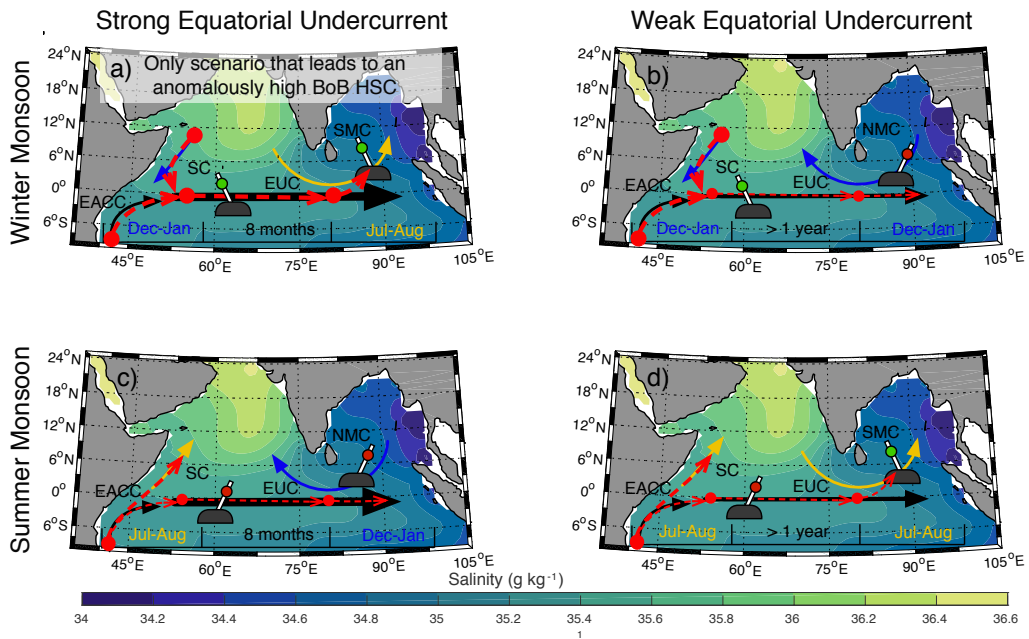


Figure 3. (a) NEMO eastward velocity (m s^{-1}) at 65°E and (b) salinity (g kg^{-1}) at 7°N; (c) Eastward velocity at 65°E averaged over 2°S to 1.5°N (blue line), salinity at 7°N averaged over 82°E to 96°E (orange line) and TropFlux zonal wind stress averaged over 2°S-2°N and 60°E-90°E (purple line); (d) Eastward velocity at 65°E (blue line), the Dipole Mode Index (DMI; yellow line) and El Niño Southern Oscillation (ENSO; green line); (e) Annual average of the spring (Feb-May) eastward velocity at 65°E (blue line) and the summer (Jun-Aug) salinity at 7°N (orange line); (f) lag correlation plots of eastward velocity at 65°E and DMI (yellow line), and eastward velocity at 65°E and ENSO (green line), where positive values indicate DMI and ENSO lead eastward velocity 65°E, and dashed lines represent statistical significance at the 95% level. All data sets have been smoothed with a 61-day moving average and time series are normalized by their standard deviation.

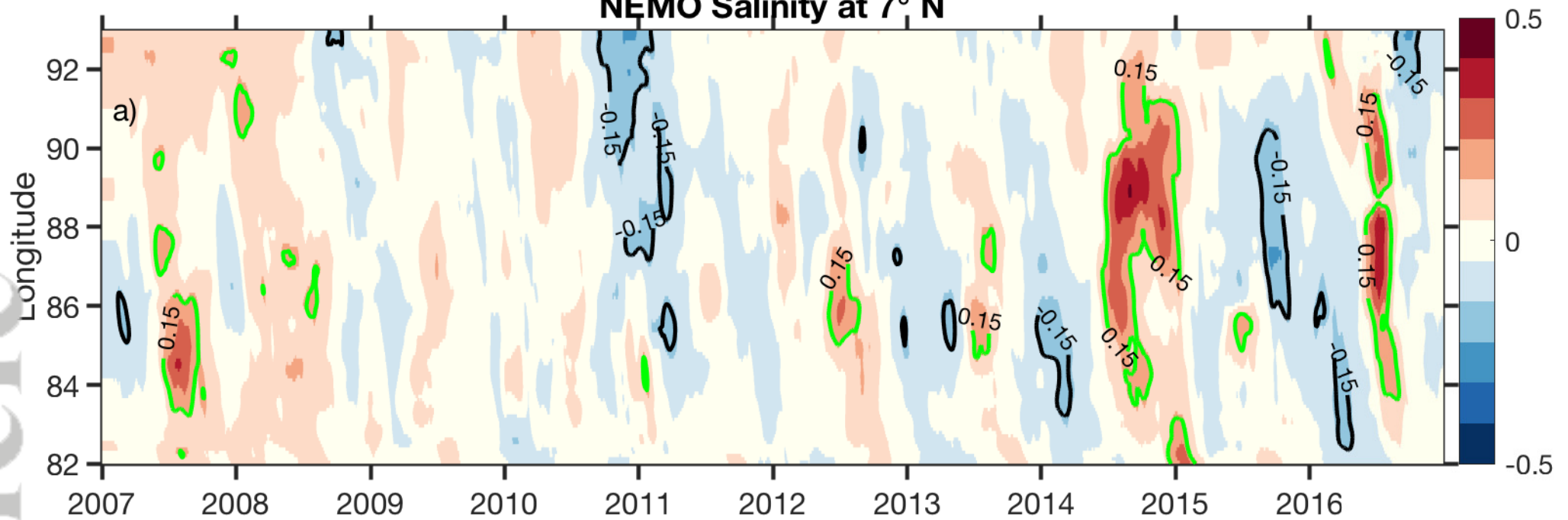


352 **Figure 4.** Railroad Switch schematic on subsurface (90 m) salinity climatology (psu; shaded)
 353 from the Argo OI product for the 4 Equatorial Undercurrent scenarios: (a,b) winter monsoon and
 354 strong (weak) Equatorial Undercurrent, and (c,d) summer monsoon and strong (weak) Equatorial
 355 Undercurrent. Red dashed arrows indicate high salinity advection.

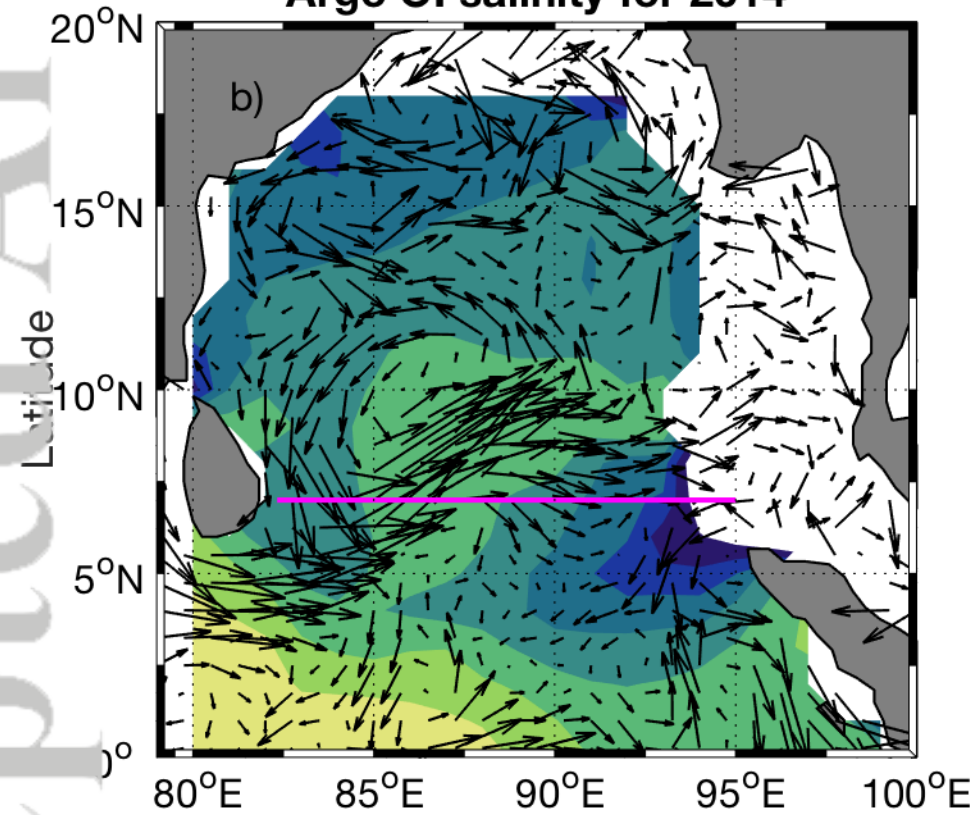
Figure 1.

Accepted Article

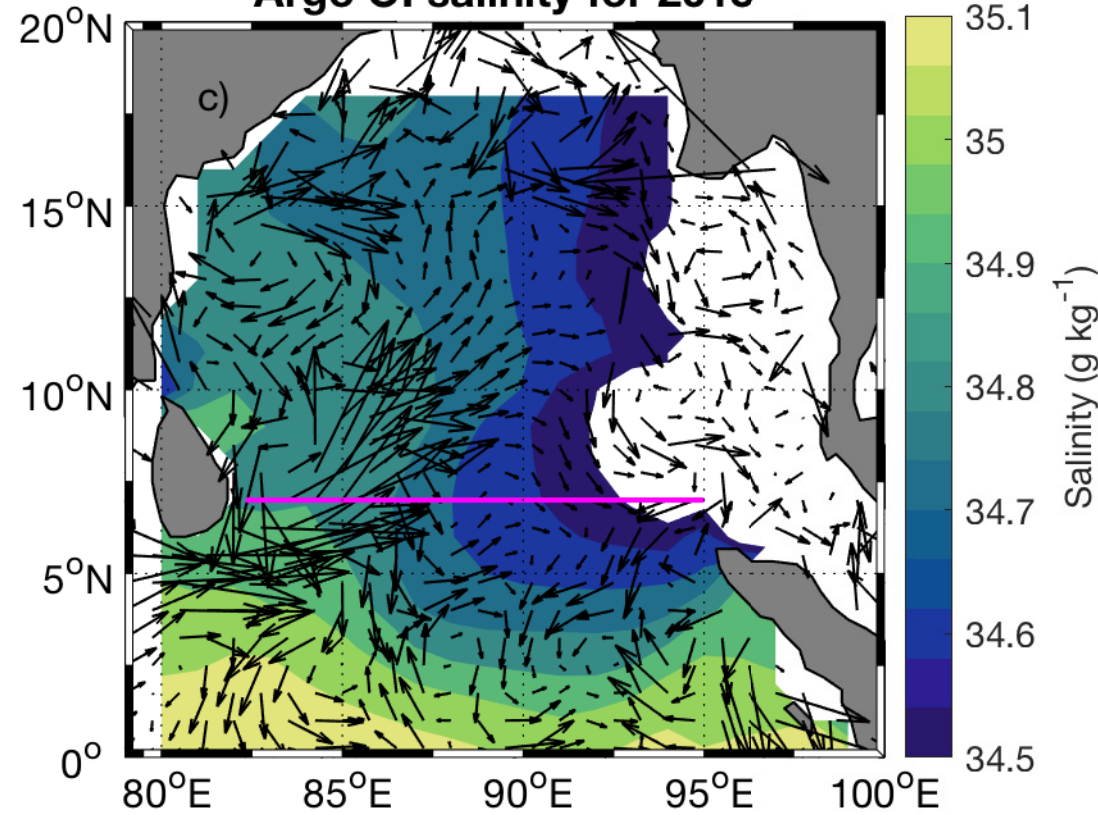
NEMO Salinity at 7° N



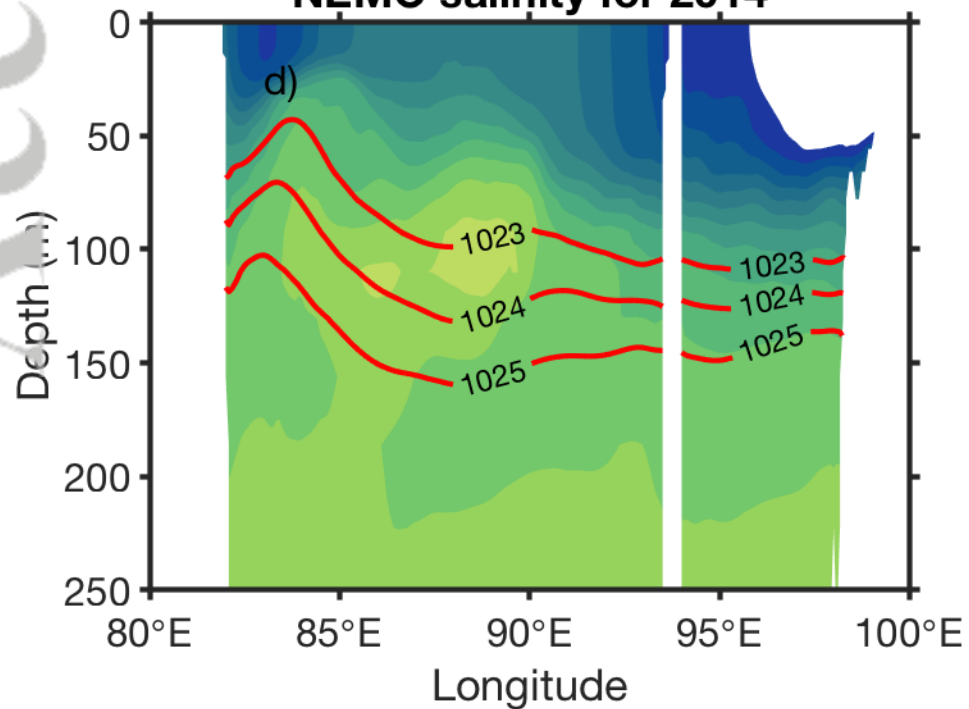
Argo OI salinity for 2014



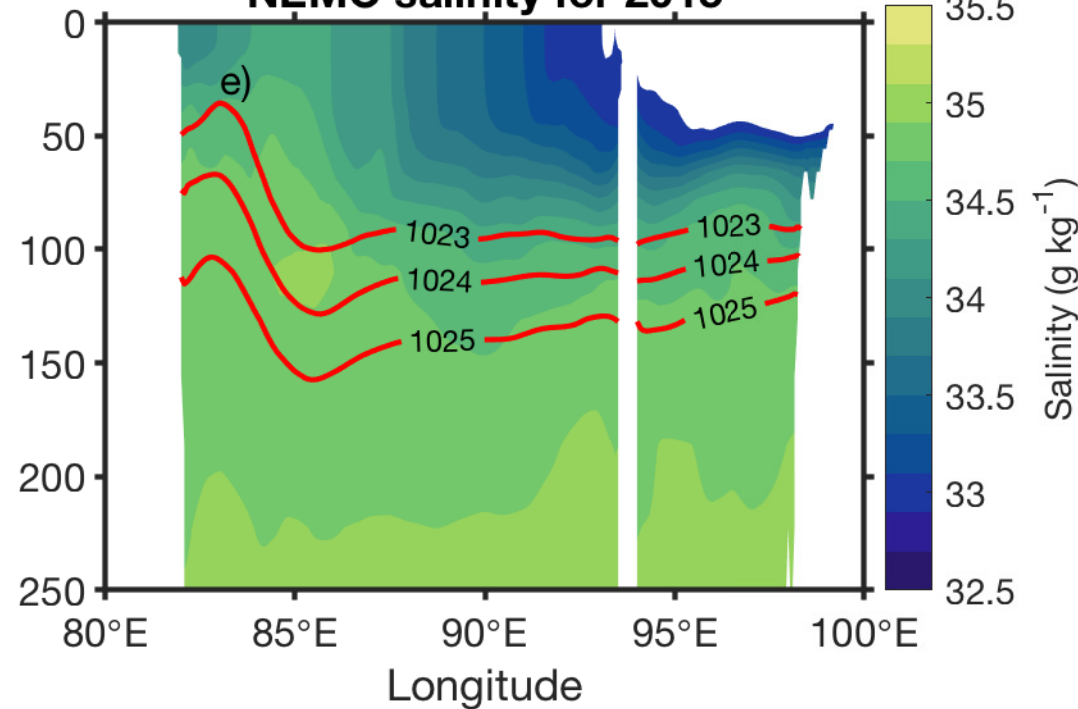
Argo OI salinity for 2015



NEMO salinity for 2014



NEMO salinity for 2015



Accepted Article

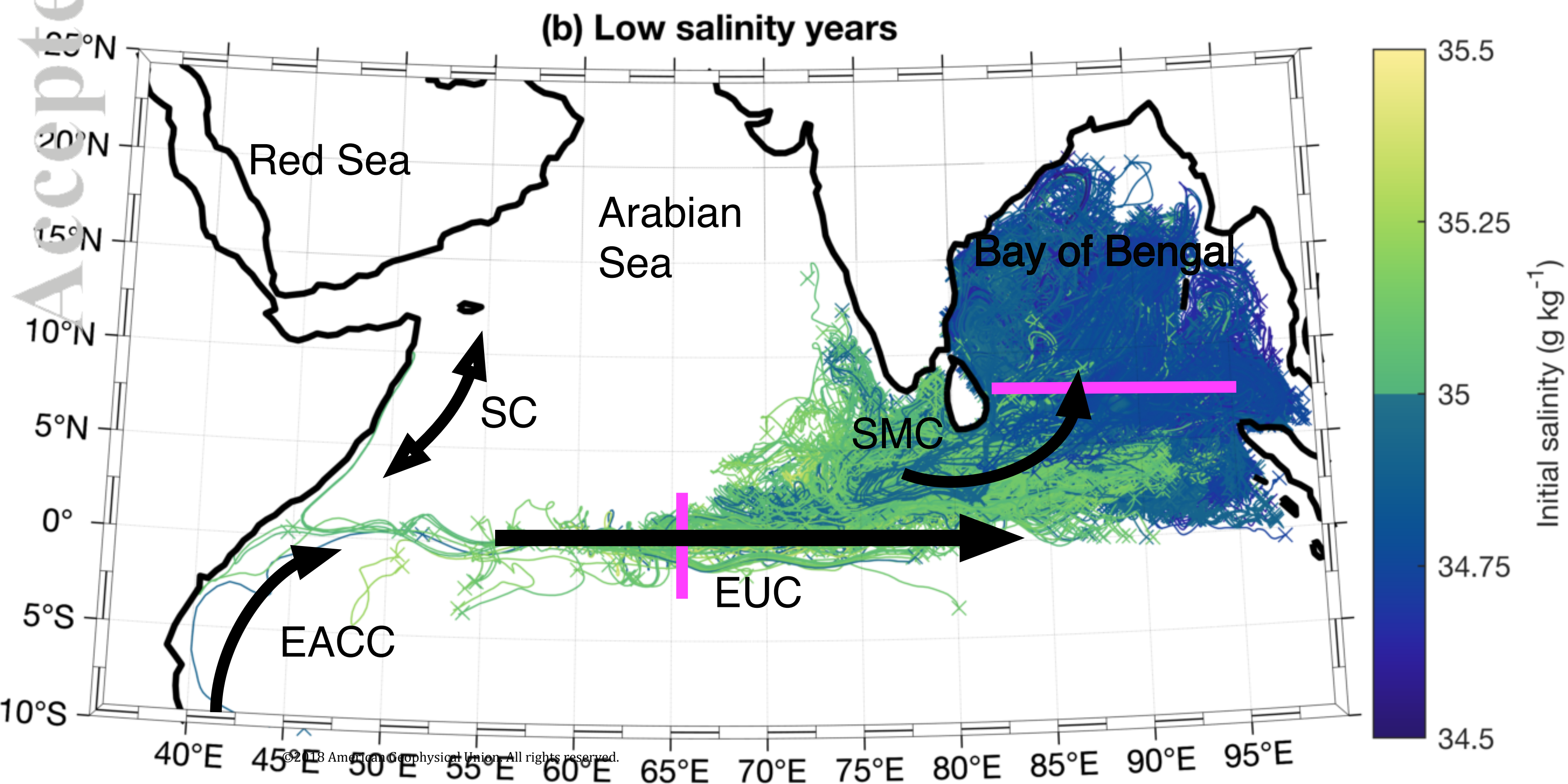
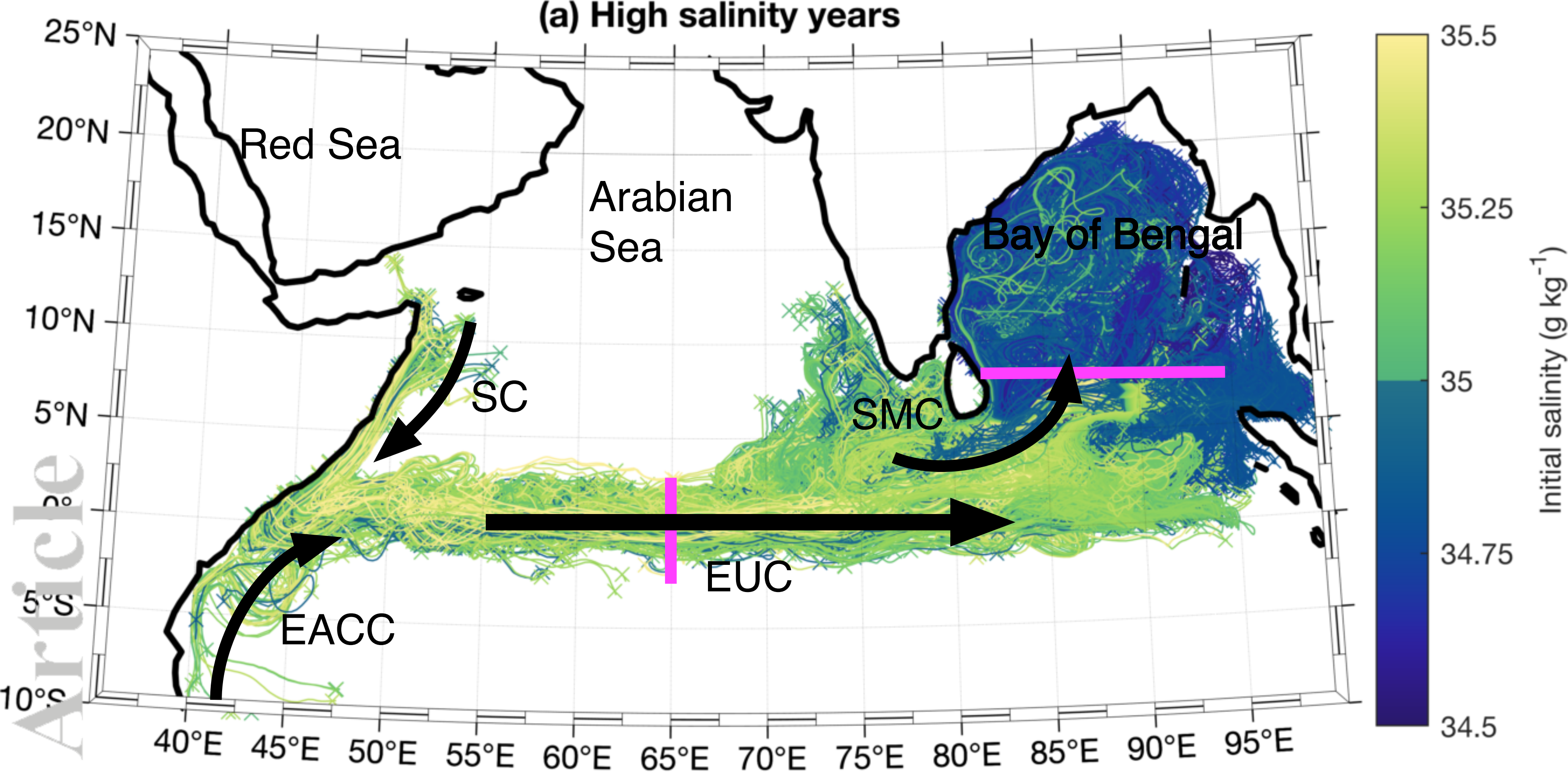
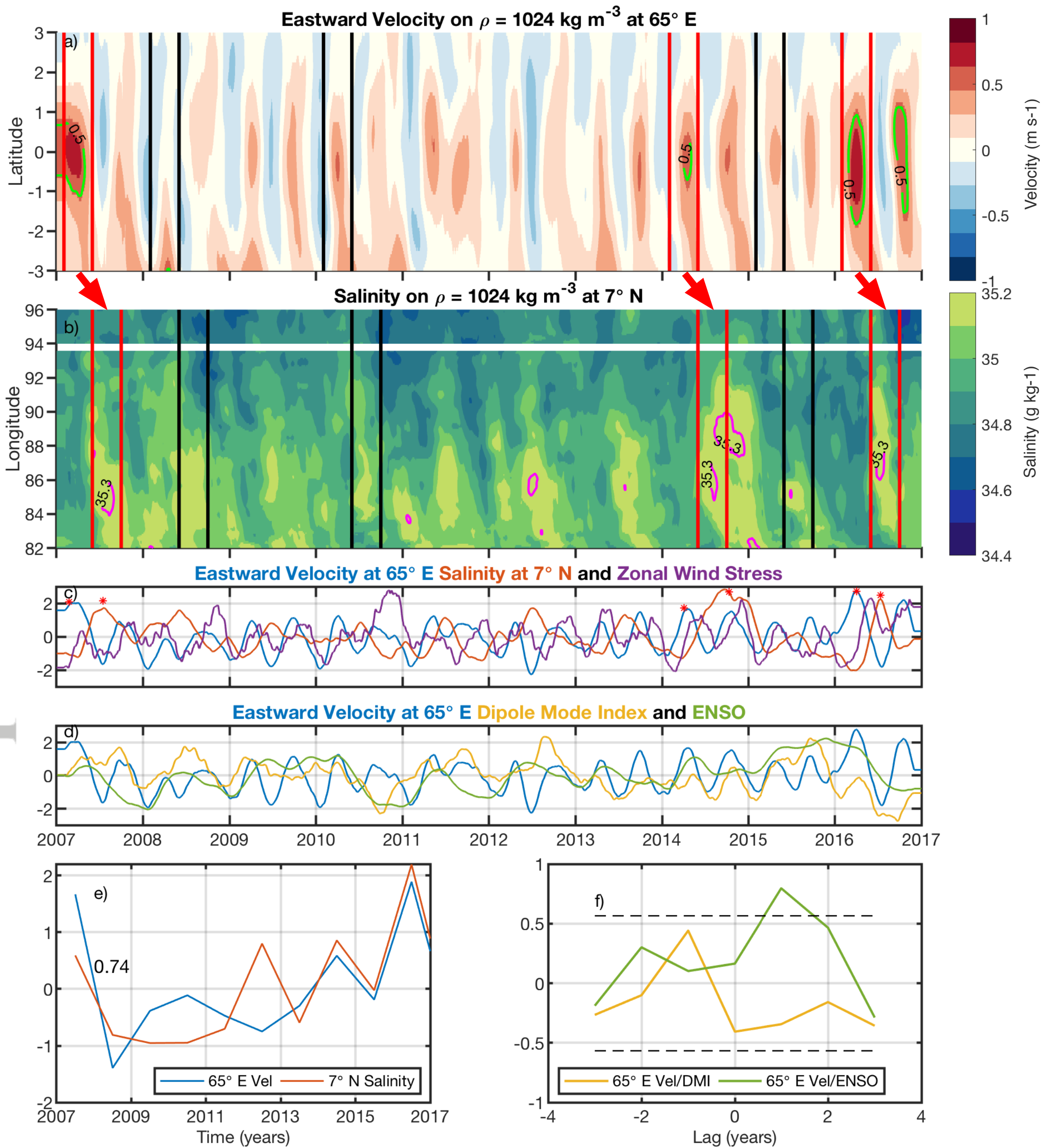


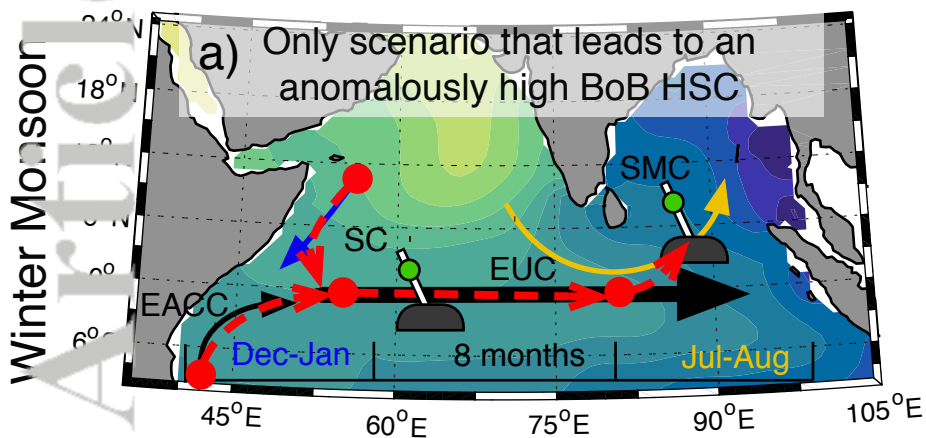
Figure 3.

Accepted Article

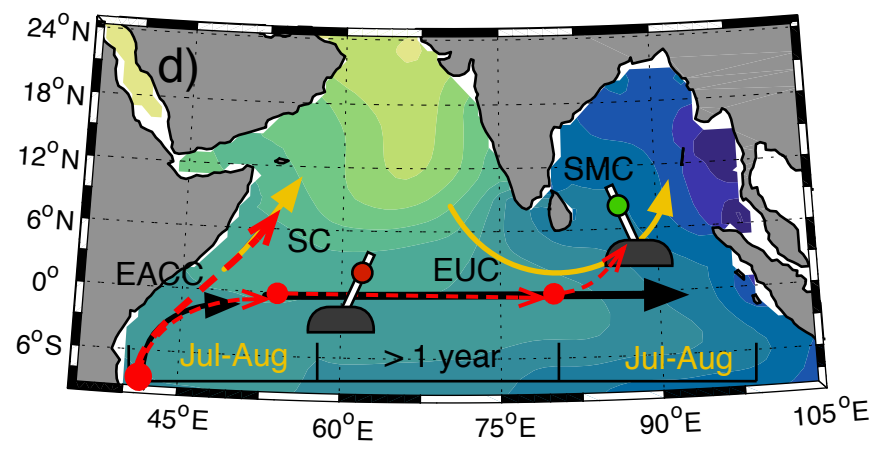
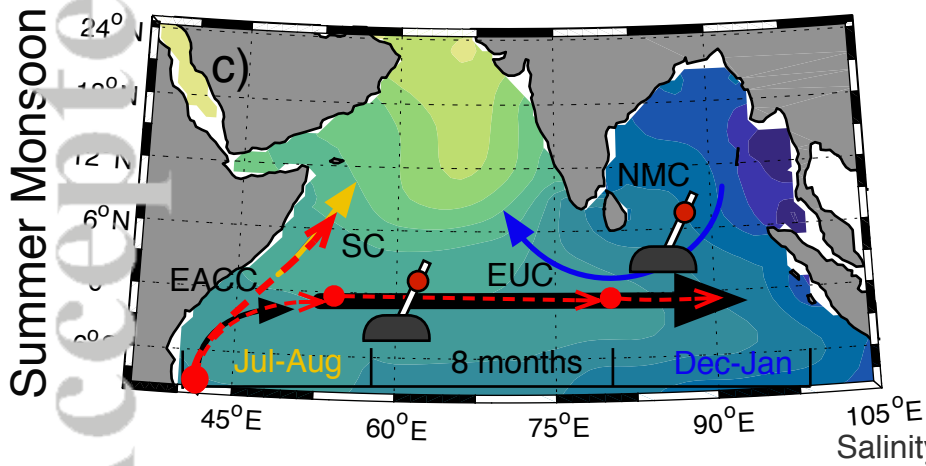
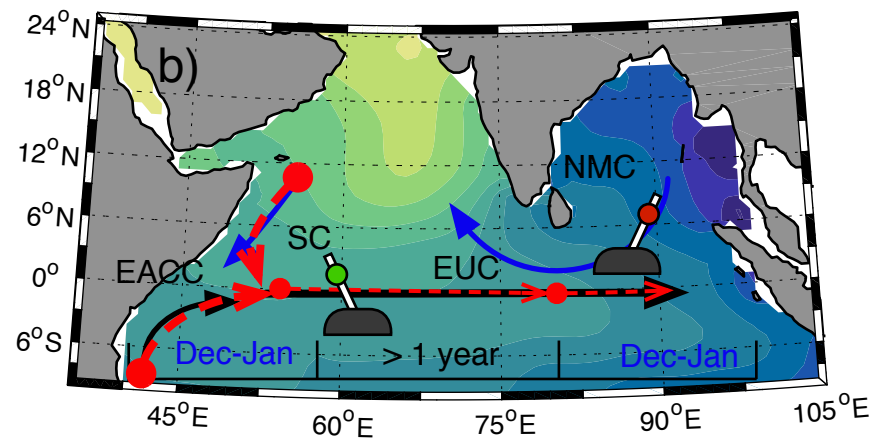


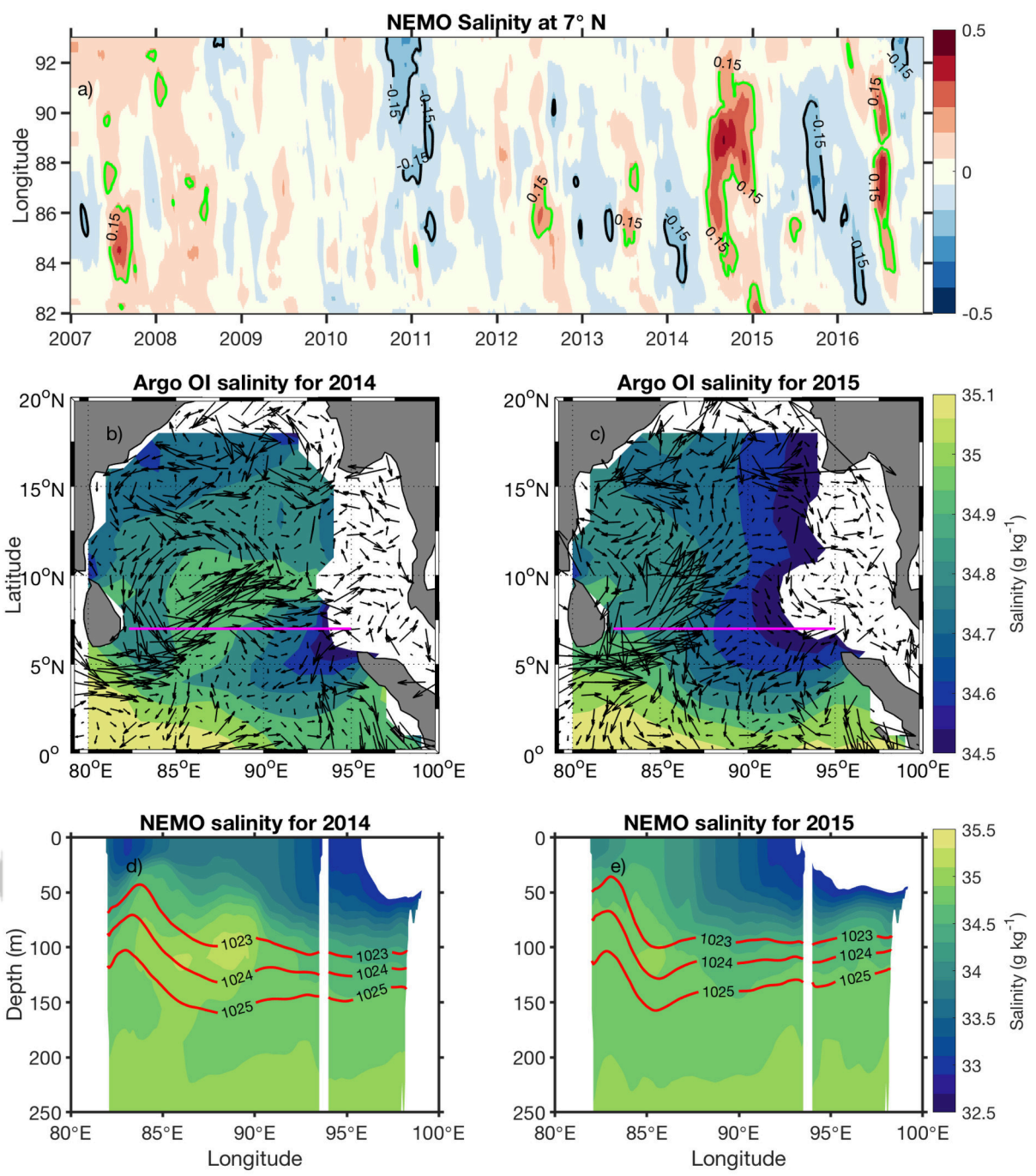
Accepted Article

Strong Equatorial Undercurrent

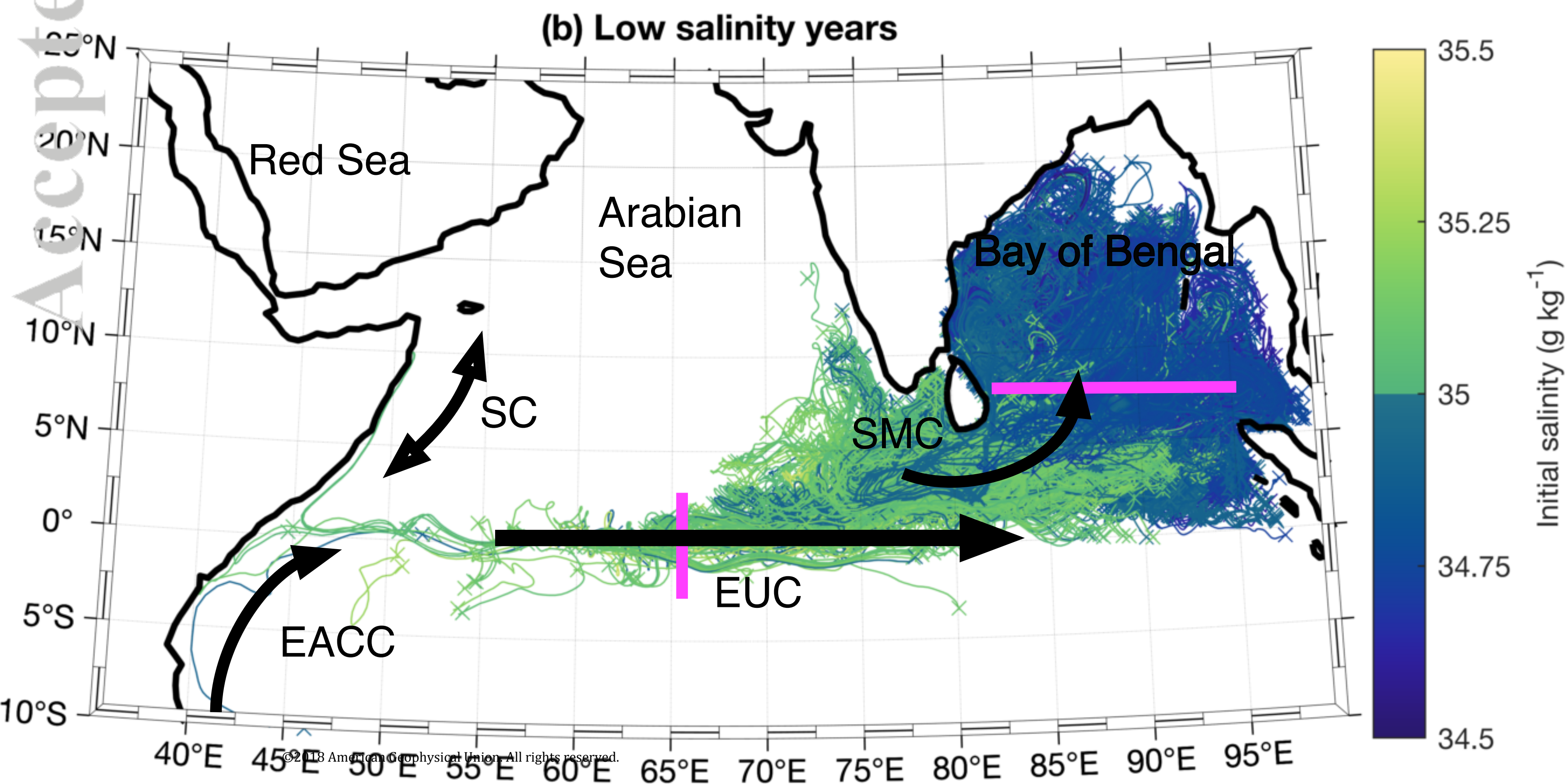
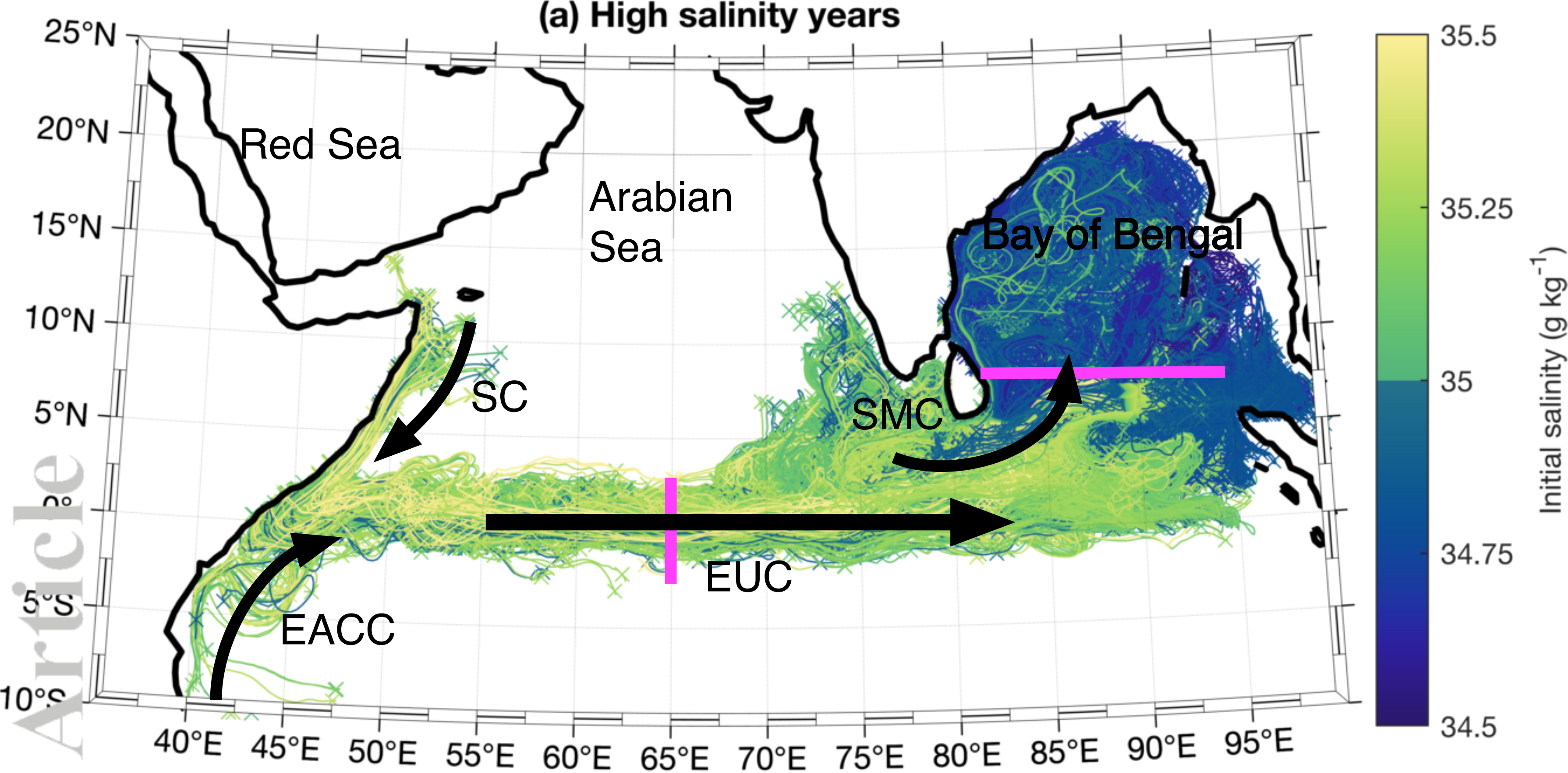


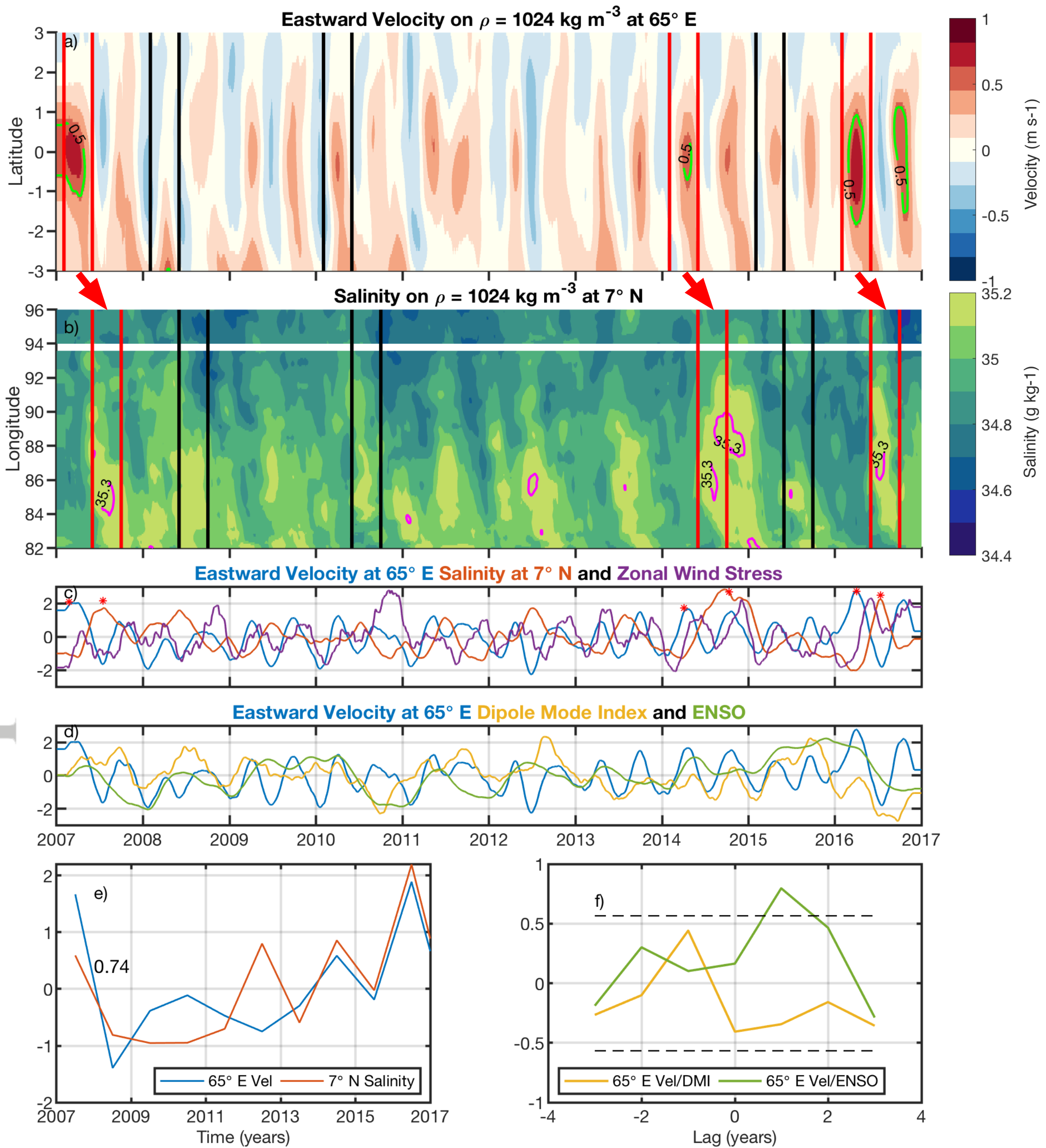
Weak Equatorial Undercurrent



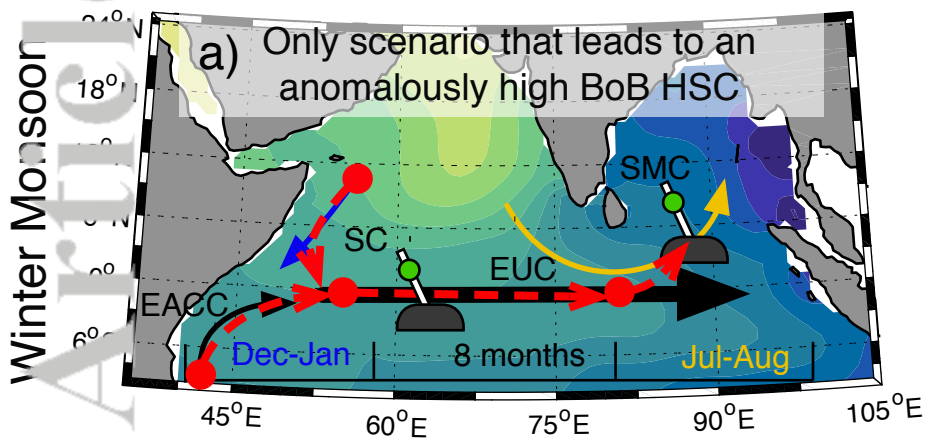


2019gl082208-f01-z-eps





Strong Equatorial Undercurrent



Weak Equatorial Undercurrent

